Sacrificial-Post Templating Method for Block Copolymer Self-Assembly

Citation: Tavakkoli K. G., Amir, Samuel M. Nicaise, Adam F. Hannon, Kevin W. Gotrik, Alfredo Alexander-Katz, Caroline A. Ross, and Karl K. Berggren. "Sacrificial-Post Templating Method for Block Copolymer Self-Assembly." Small 10, no. 3 (July 10, 2013): 493–499.

As Published: http://dx.doi.org/10.1002/smll.201301066

Publisher: Wiley Blackwell

Persistent URL: http://hdl.handle.net/1721.1/92711

Version: Author's final manuscript: final author's manuscript post peer review, without publisher's formatting or copy editing

Sacrificial-Post Templating Method for Block Copolymer Self-Assembly

Amir Tavakkoli K. G. [*], *Samuel M. Nicaise*[*], *Adam F. Hannon, Kevin W. Gotrik, Alfredo Alexander-Katz, Caroline A. Ross, Karl K. Berggren*[**]

[*] These authors contributed equally to the reported work.
[**] Dr. A. Tavakkoli K. G., S. M. Nicaise, Prof. K. K. Berggren
Department of Electrical Engineering and Computer Science,
Massachusetts Institute of Technology,
Cambridge, MA 02139, USA
E-mail: berggren@mit.edu
Dr. A. Tavakkoli K. G.
NUS Graduate School for Integrative Sciences & Engineering (NGS),
Singapore 117456
A. F. Hannon, K. W. Gotrik, Prof. A. Alexander-Katz, Prof. C. A. Ross
Department of Materials Science and Engineering,
Massachusetts Institute of Technology,
Cambridge, MA 02139, USA

Supporting Information is available under http://www.small-journal.com or from the author.

Keywords: sacrificial-post template, block copolymer directed self-assembly, bimodal size distribution, nanostructure, square and hexagonal lattice

A sacrificial-post templating method is presented for directing block copolymer self-assembly to form nanostructures consisting of monolayers and bilayers of microdomains. In this approach, the topographical post template is removed after self-assembly and therefore is not incorporated into the final microdomain pattern. Arrays of nanoscale holes of different shapes and symmetries, including mesh structures and perforated lamellae with a bimodal pore size distribution, are produced. The ratio of the pore sizes in the bimodal distributions can be varied via the template pitch, and agrees with predictions of self consistent field theory.

1. Introduction

Numerous studies have shown that it is possible to direct the microphase separation in block copolymer (BCP) thin films using chemical or physical templating methods to produce a monolayer or a bilayer of microdomains with complex and well-ordered nanostructures.[1]–[18] In particular, topographical templating using nanoscale posts has been shown to promote a range of non-bulk morphologies from a given BCP and to produce pattern density

multiplication in which the areal density of microdomains exceeds that of the templating features.[19,20] In general, for topographical templating the template becomes incorporated into the BCP microdomain array. Sacrificial methods have therefore been developed to direct BCP self-assembly in trenches made from an etchable material, allowing the subsequent removal of the template to result in a template-free final arrangement of microdomains.[21,22]

This article presents a sacrificial-post templating method for BCP self-assembly which combines the capabilities of post templating with the sacrificial templating methods developed for trench topographies. The method described here produces geometries previously not realized by physical or chemical templating such as 3-D grid patterns and arrays of holes with bimodal size distributions. Furthermore, sacrificial-post templating is expected to be integrable with semiconductor manufacturing processes because the templates could possibly be made using optical lithography and trim etching (instead of the electron-beam lithography presented in this work).[23] The use of a removable template could mitigate potential pattern transfer difficulties caused by the dissimilar etch rates for physical templates compared to the BCP nanopatterns.

Prior work has demonstrated the use of removable templates with feature sizes that are coarse compared with the period of the BCP. Ilievski *et al.*[21] used trenches made from an anti-reflective coating (ARC) for graphoepitaxy of spherical-morphology poly(styrene-block-ferrocenyldimethylsilane). The ARC was subsequently removed by O_2 plasma etching along with the polystyrene block to leave only the templated polyferrocenyldimethylsilane microdomains. Moon *et al.*[22] made removable templates using deep-UV lithography to template lamellar poly(styrene-block-methyl methacrylate), then followed the template removal by infilling the spaces formerly occupied by the template with a second BCP thin film templated by the first BCP pattern. Several reports showed the fabrication of BCP nanopatterns from reusable nanoimprint trench templates.[24–26] These imprint processes

generated highly oriented patterns, and the patternless regions could subsequently be filled by additional steps.[22,27]

Post templating makes use of arrays of posts with lateral dimensions on the order of half the period of the BCP to create a range of complex microdomain patterns including several morphologies on a single substrate and bilayer meshes not achievable using trench templates.[19,20] However, the posts have been made from an inorganic resist material, hydrogen silsesquioxane (HSQ), which is etch resistant. By making the posts from an organic resist, polymethylmethacrylate (PMMA), the posts can be removed along with the polystyrene block of a polystyrene-polydimethylsiloxane (PS-*b*-PDMS) BCP using an oxygen etch, leaving only the PDMS microdomains behind. We demonstrate here the templating of PDMS nanostructures including in-plane cylinders, spheres, ellipsoids, and superstructures; perforated lamellae and rectangular meshes with holes of different diameters, symmetries (square and hexagonal), shapes (square, circular, rectangular and hexagonal) and bimodal hole sizes; and with two- and three-fold pattern multiplication, expanding on previous results.[20] The experimental results for the bimodal size distribution and pattern multiplication gave excellent agreement with self-consistent field theory (SCFT) models. For applications such as stepper mask generation and high-density magnetic storage which rely on electron-beam lithography for pattern generation, this technology could increase throughput, process latitude, and pattern variety. Furthermore, BCP directed self-assembly is applicable in areas such as integrated circuits,[28] nanowire transistors,[29] cell analysis,[30] gas sensing,[31] and magnetic nanopatterns for data storage. [32,33]

2. Experimental procedure

Figure 1 shows the major steps of the sacrificial-post templating method for the fabrication of monolayers (Figure 1, top) and bilayers (Figure 1, bottom) of microdomains from a PS-*b*-PDMS BCP in which the bulk morphology consisted of cylinders of PDMS in a PS matrix. In the first step, the templates were fabricated using electron-beam-lithography

(EBL) exposure of PMMA resist on a silicon substrate. Next, the templates were chemically functionalized with a hydroxyl-terminated PS brush and the PS-*b*-PDMS was spin-coated onto the substrates. BCP films were annealed at room temperature in a cosolvent vapor consisting of 5 parts toluene to 1 part heptane.[34] An oxygen reactive ion etch (RIE) was used to remove the PS block and leave the oxidized-PDMS (ox-PDMS) patterns on the substrates. A variety of mono- and bilayer structures was achieved using template patterns with different lattices, periods, and diameters of the posts.

The templates were fabricated using EBL of 40 nm thick films of PMMA as a negative-tone resist (Figure 1, Step 1). PMMA is typically a positive-tone resist but previous studies have shown that this resist acts as a negative-tone resist due to a carbonization process when exposed to doses about 30 times the positive-tone dose and developed with methyl isobutyl ketone (MIBK).[35] When PMMA is highly dosed, there are three regions with respect to the beam spot: a highly exposed region near the beam spot from the primary beam and secondary electrons; a lightly exposed region in proximity to the beam spot from the backscattered electrons; and an unexposed region far from the beam spot. Development with MIBK only removed the PMMA from the lightly exposed region,[35] and failed to remove the PMMA from the unexposed region, so the process was modified by sonicating the samples in acetone for 2 min after development. Acetone sonication removed the unexposed PMMA and left the posts on the substrates (see Figure S2 as an example of a PMMA-post template).

After the exposure and development, the diameter and the height of the posts were about 17-30 nm and 30 nm, respectively (see Experimental Section for more details of the PMMA-template fabrication). Next, the samples were functionalized with hydroxyl-terminated PS brush, PS-OH (1 kg mol^{-1}, purchased from PolymerSource, Canada), by spin-coating the PS-OH then annealing for 14 hrs under vacuum at 170°C (Figure 1, Step 2), which made the posts repulsive to the minority block (PDMS) and attractive to the majority block (PS). PS-*b*-PDMS (MW=45.5 kg mol^{-1}, f_{PDMS}=0.32, equilibrium period approximately 35 nm,

2 wt% in PGMEA solvent, purchased from Polymer Source) was spin-coated onto substrates to an average thickness of 30 nm in order to achieve a monolayer of in-plane PDMS cylindrical microdomains on untemplated substrates, and 42 nm thick to obtain bilayers of cylinders. Solvent annealing was carried out using the vapor from a volumetric mixture of toluene and heptane (5:1), a ratio which helped control the microdomain size of PDMS, for 1.5 hrs at room temperature (Figure 1, Step 3).[36] A CF_4 RIE was used to remove the PDMS surface wetting layer, immediately followed by an O_2 RIE to simultaneously remove the PS matrix and the PMMA posts and to oxidize the PDMS, leaving the final ox-PDMS nanopatterns on the surface (Figure 1, Step 4).

3.Results and discussion

3.1. Monolayer microdomain morphologies vs. post spacing

Figures 2 and S3-S5 show the experimental results of the fabrication of monolayer structures using the sacrificial-post templating method. The middle of the image shows regions where the sacrificial-posts were patterned whereas the left and right sides of the images, which were covered with randomly oriented in-plane cylinders, are representative of unpatterned areas. Insets in these figures show the locations of PMMA posts before removal by the O_2 RIE.

The microdomains of the BCP transitioned between multiple morphologies as a function of the post pitch. For example, increasing the pitch for a square or rectangular symmetry post array resulted in in-plane cylinders (Figure S4.c) transitioning to spheres (Figure 2.a and S5), ellipsoids (Figure S4.a), periodic superstructures (Figure S4.b), perforated lamellae labeled L1 where each post corresponds to one hole (Figures 2.b, S3) and perforated lamellae with additional generated pores that appeared in between the posts, labeled L2 (Figure 2.c,d). In the sphere array, Figure 2a, the PDMS spheres had similar diameter to the PMMA posts. The holes in the perforated lamellae were not necessarily circular, e.g. Figures 2b and 2c show holes with a rounded square shape. Hexagonal post

arrays also led to L1 and L2 perforated lamellae with hexagonal symmetry (Figures S3 and 2d). These transitions are driven by changes in commensurability between the post spacing and BCP period, and are the same as those obtained from HSQ posts.[20] This shows that the PS-brush effectively attached to the PMMA posts and provided the same boundary conditions as those obtained from PS-functionalized HSQ posts. Characterization of the attaching of an OH-terminated brush onto PMMA is described further in SI, Section 1.

3D SCFT simulations were performed to gain insight into the effect of post pitch on the morphology, shape and size of the experimental nanostructures.[20] **Figure 3** shows simulation results analogous to the nanopatterns achieved in Figure 2 which were produced by changing the ratio between the post spacing and L_0, the BCP equilibrium period. These simulation results are based on a unit cell containing one or two posts and periodic boundary conditions, in which the posts and substrate surfaces are attractive to the majority block and the top (air) surface to the minority block. Details of the model are given in Ref. 20 and in the SI, section 4. In the case of the structures in Figure 3.a,b,c, the square symmetry of the PDMS microdomains is driven by the square symmetry of the post array with period $<2L_0$, which provides a strong templating effect similar to previous work with square symmetry chemical patterns that promoted square symmetry arrays of cylindrical microdomains.[14,20] The SCFT reproduced the trend in morphology from spheres to L1 and then L2 as seen experimentally with increasing template pitch, and also showed that the curvature and the shape of the hole produced around the posts was non-circular.

3.2. Perforated lamellar morphologies (L2)

The perforated lamellar structures L2 are of particular interest because of the density multiplication of the holes compared to the posts, and because bimodal hole sizes can be produced. This structure was observed in prior work using HSQ posts,[20] but the trends in hole size were not analyzed. Figures S6 and S7 show examples of L2 structures produced from HSQ posts, which are similar to Figure 2.c,d produced from PMMA posts. In each case,

two types of holes were identified: post-holes, which surrounded the posts, and generated-holes which formed between the posts. In Figure 2.c,d, each post generated an additional one and two holes, respectively.

Figure 4 shows how the sizes of the post-holes and generated-holes varied with the post pitch and diameter for the hexagonal symmetry L2 perforated lamella of Figure 3d. Here the post pitch is the center-to-center distance between posts. A Matlab computer program was used to extract the experimental data points presented in Figure 4 from SEM images (See SI, Section 4 for more details). The simulated data points were determined from only those simulations which formed the L2 structure. The coarse-graining limited the values of post spacing and diameter that could be modeled. The post diameter in the simulation was changed by increments of ~3 nm. However, the simulations examined a wider range of post pitches and post diameters than the experiment, up to 110 nm (~3.2L_0) and 43 nm (~1.2L_0), respectively, where L_0 is the cylinder spacing in the untemplated BCP, ~35 nm. Out of 12 simulations, 4 had defects in which two of the generated-holes connected. These data points are shown with a hollow triangle or square in the plot, and such defects were observed experimentally as well.

Figure S8 shows the range of post spacings and diameters that produced L2 structures. The L2 structure formed in templates with an interpost spacing (i.e. the difference between post pitch and post diameter) of approximately 2L_0 over a range of post pitches and diameters.

The general experimental observation was that the generated-holes had an approximately constant diameter, whereas the post-hole diameter increased with post pitch and post diameter, giving a bimodal hole size distribution. The post-holes were formed by the PS chains which surrounded each post, and their diameter therefore increased (linearly) as the posts became larger. In contrast, the generated-holes had an almost invariant diameter similar to that formed in an untemplated perforated lamella, and there would be a large entropic penalty for the chain extension needed to increase their size. The SCFT results agreed very

well with the experimental results, and suggested that the trends in hole size would extend to larger template pitch and diameter than the experimentally investigated range.

The minimum post pitch where the L2 perforated lamella was observed was ~80 nm. If a cylindrical BCP of period L_0 were to transition into a perforated lamella, the row spacing of the holes would be L_0 and the center-to-center distance between holes would be $L_0\sqrt{3}/2$, meaning a post pitch of at least $2L_0$ (70 nm) is necessary to allow two rows of holes to fit between each pair of posts and thus stabilize the normally metastable perforated lamellae structure. This commensurate condition stabilized the hexagonal L2 structure, which persisted to post pitches of at least 3.2 L_0 (in the model) = 110 nm by accommodating the strain through increases in the post-hole diameter. The post template helps to stabilize the normally metastable perforated lamella due to the confinement effects.[37–40]

3.3. Bilayer microdomain arrays

Figure 5 shows the results of the bilayer mesh-shaped nanostructures after post removal (Figure 1, step 4, bottom). The mesh-shaped structures formed from a film that was thick enough to produce a bilayer of in-plane cylinders over the region of the substrate containing posts. The mesh formed when the post pitch in the diagonal or *y*-direction was equal to L_0, favoring alignment of one layer of cylinders perpendicular to the diagonal or *y*-direction, and the post period in the *x*-direction was slightly less than an integer multiple of L_0.[19] The PMMA posts produced the same structures as HSQ posts,[19] but post removal left rectangular holes. This is in contrast to the untemplated regions of the substrate in which the upper and lower layers of cylinders were parallel without long range order. Insets in these figures show the locations of posts before removal. Figure 5.b shows bimodal rectangular holes after etching bilayer structures, templated by posts with a larger *x*-spacing.

4. Conclusions

In summary, this article demonstrates a sacrificial post-templating method which avoided the incorporation of the physical templates into final BCP nanopatterns. The

removable PMMA post array templated structures similar to those formed from an HSQ post array with the same geometry, because the majority brush layer on the posts led to the same boundary conditions on the self-assembly of the BCP irrespective of the post material. This method was successfully used for the fabrication of both monolayers of in-plane microdomains, including spheres, cylinders and perforated lamellae, and bilayers of cylinders forming a mesh structure, and pattern density multiplication was achieved. Perforated lamellae with bimodal hole sizes were analysed in detail, showing that the set of holes formed by density multiplication had a diameter that was almost independent of template geometry while the other set of holes formed around the posts had a diameter that increased with post diameter. These results are expected to simplify pattern transfer in BCP lithography, and provide a route to making hole arrays with bimodal size distribution and square, rectangular or hexagonal symmetries.

5. Experimental Section

Template fabrication: In the first step, prime silicon (100) wafers were cut into pieces ~ 2 cm × 2 cm and diluted PMMA was spin-coated onto the pieces. The PMMA (950 kg/mol in anisole purchased from MicroChem Corp.) was diluted with a volumetric dilution ratio of about 1:8 PMMA:anisole. To produce 40 nm thickness films (measured by ellipsometer), a 4000 rpm spin coating speed was used. To evaporate the additional solvent and improve the adhesion between the PMMA resist and the substrate, the samples were baked on a hot plate at 200°C for 2 min. A Raith 150 scanning electron beam lithography system was used at a 30 keV accelerating voltage, about 240 pA beam current, and a 6 mm working distance to expose the PMMA resist. 434-1240 fC/dot dose range was used for exposing square and hexagonal arrays of dots. After exposure, the substrates were developed in methyl isobutyl ketone (MIBK) for 2 min and rinsed in isopropanol (IPA) for 1 min. MIBK could only remove the lightly exposed PMMA but not the unexposed PMMA, so the samples were sonicated in acetone for 2 min (post-MIBK-development) to completely remove the unexposed PMMA

and leave PMMA posts on the substrates (Figure S2). The diameter of the PMMA posts was 17-30 nm and their height was around 30 nm. A Raith 150 with an accelerating voltage of 10 keV and a working distance of 6 mm was used for imaging.

Block copolymer self-assembly: Solvent vapor annealing (SVA) was used to facilitate the self-assembly of the BCP thin films. This was done using a simple beaker setup where a crystallization dish (1.5 cm in height, 5 cm in diameter) was used to contain the solvent and the thin film. The thin film was placed on a glass platform 0.6 cm from the base of the dish and 1.5 ml of a toluene and heptane mixture (5:1 toluene:heptane by volume) was placed in the chamber. The chamber was capped using a 10cm glass petri dish which was placed over the top. The dish did not completely close off the solvent vapor from the environment, so leakage occurred at a rate of 590 μg/min as measured by tracking the mass of the system versus time. CF_4 RIE etching was done at a power of 50 W, a flow of 15 sccm and pressure of 15 mTorr. 5 seconds of etching removed the top-layer PDMS block. O_2 RIE etching was done at a power of 90 W, a flow of 10 sccm, and pressure of 6 mTorr. 22 seconds of etching removed the PS majority block and PMMA templates.

Acknowledgements

The authors acknowledge support from the Semiconductor Research Corporation, the FENA Center, NRI, SMA, National Science Foundation, Tokyo Electron and Taiwan Semiconductor Manufacturing Company. A.T.K.G would like to express his sincere gratitude to T. C. Chong and S. N. Piramanayagam for their support. A.T.K.G and S.M.N. acknowledge their fellowships from NGS Singapore and NSF, respectively. The Research Laboratory of Electronics Scanning-Electron-Beam Lithography Facility provided facilities for this work. The authors also thank M. Mondol, J. Daley, V. Manfrinato and members of Computer Vision Research Group at MIT CSAIL and L. Shaw at MIT CMSE Surface Analysis for technical assistance. A U.S. Patent titled “Removable Templates for Directed Self-assembly” has been filed.

[1] J. K. Bosworth, M. Y. Paik, R. Ruiz, E. L. Schwartz, J. Q. Huang, A. W. Ko, D. M. Smilgies, C. T. Black, and C. K. Ober, *ACS Nano*, **2008**, *2*, 1396.

[2] S. Park, D. H. Lee, J. Xu, B. Kim, S. W. Hong, U. Jeong, T. Xu, and T. P. Russell, *Science*, **2009**, *323*, 1030.

[3] Y. Wu, G. Cheng, K. Katsov, S. W. Sides, J. Wang, J. Tang, G. H. Fredrickson, M. Moskovits, and G. D. Stucky, *Nature Mat.*, **2004**, *3*, 816.

[4] R. A. Segalman, A. Hexemer, and E. J. Kramer, *Macromol.*, 2003, 36, 6831.

[5] J. K. . Yang, Y. S. Jung, J. B. Chang, R. A. Mickiewicz, A. Alexander-Katz, C. A. Ross, and K. K. Berggren, *Nature Nanotech.*, **2010**, *5*, 256.

[6] R. Ruiz, H. Kang, F. A. Detcheverry, E. Dobisz, D. S. Kercher, T. R. Albrecht, J. J. de Pablo, and P. F. Nealey, *Science*, **2008**, *321*, 936.

[7] J. Y. Cheng, C. T. Rettner, D. P. Sanders, H.-C. Kim, and W. D. Hinsberg, *Adv. Mat.*, **2008**, 20, 3155.

[8] S. O. Kim, H. H. Solak, M. P. Stoykovich, N. J. Ferrier, J. J. De Pablo, P. F. Nealey, and others, *Nature*, **2003**, *424*, 411.

[9] I. Bita, J. K. . Yang, Y. S. Jung, C. A. Ross, E. L. Thomas, and K. K. Berggren, *Science*, **2008**, *321*, 939.

[10] J. Y. Cheng, C. A. Ross, E. L. Thomas, H. I. Smith, and G. J. Vancso, *Adv. Mat.*, **2003**, *15*, 1599.

[11] S. Ji, U. Nagpal, W. Liao, C. C. Liu, J. J. de Pablo, and P. F. Nealey, *Adv. Mat.*, **2011**, *23*, 3692.

[12] S. M. Park, G. S. W. Craig, Y. H. La, and P. F. Nealey, *Macromol.*, **2008**, *41*, 9124.

[13] K. C. Daoulas, M. Müller, M. P. Stoykovich, S. M. Park, Y. J. Papakonstantopoulos, J. J. de Pablo, P. F. Nealey, and H. H. Solak, *Phys. Rev. Lett.*, **2006**, *96*, 36104.

[14] S. M. Park, G. S. W. Craig, Y. H. La, H. H. Solak, and P. F. Nealey, *Macromol.*, **2007**, *40*, 5084.

[15] H. Jung, D. Hwang, E. Kim, B. J. Kim, W. B. Lee, J. Poelma, J. Kim, C. J. Hawker, J. Huh, D. Y. Ryu, and J. Bang, *ACS Nano*, **2011**, *5*, 6164.

[16] F. Rose, J. K. Bosworth, E. A. Dobisz, and R. Ruiz, *Nanotech.*, **2011**, *22*, 035603.

[17] E. Kim, C. Shin, H. Ahn, D. Y. Ryu, J. Bang, C. J. Hawker, and T. P. Russell, *Soft Matter*, **2008**, *4*, 475.

[18] K. Shin, H. Xiang, S. I. Moon, T. Kim, T. J. McCarthy, and T. P. Russell, *Science*, **2004**, *306*, 76.

[19] A. Tavakkoli K. G., K. W. Gotrik, A. F. Hannon, A. Alexander-Katz, C. A. Ross, and K. K. Berggren, *Science*, **2012**, *336*, 1294.

[20] A. Tavakkoli K. G., A. F. Hannon, K. W. Gotrik, A. Alexander-Katz, C. A. Ross, and K. K. Berggren, *Adv. Mat.*, **2012**, *24*, 4249.

[21] F. Ilievski and C. A. Ross, *J. Vac. Sci. & Tech. B.*, **2010**, *28*, 42.

[22] H. S. Moon, D. O. Shin, B. H. Kim, H. M. Jin, S. Lee, M. G. Lee, and S. O. Kim, *J. Mat. Chem.*, **2012**, *22*, 6307.

[23] J. W. Jeong, W. I. Park, L. M. Do, J. H. Park, T. H. Kim, G. Chae, and Y. S. Jung, *Adv. Mat.*, **2012**, *24*, 3526.

[24] S. M. Park, X. Liang, B. D. Harteneck, T. E. Pick, N. Hiroshiba, Y. Wu, B. A. Helms, and D. L. Olynick, *ACS Nano*, **2011**, *5*, 8523.

[25] V. S. D. Voet, T. E. Pick, S. M. Park, M. Moritz, A. T. Hammack, J. J. Urban, D. F. Ogletree, D. L. Olynick, and B. A. Helms, *J. Am. Chem. Soc.*, **2011**, *133*, 2812.

[26] S. J. Jeong, H. S. Moon, B. H. Kim, J. Y. Kim, J. Yu, S. Lee, M. G. Lee, H. Y. Choi, and S. O. Kim, *ACS Nano*, **2010**, *4*, 5181.

[27] M. P. Stoykovich, H. Kang, K. C. Daoulas, G. Liu, C.-C. Liu, J. J. de Pablo, M. Müller and P. F. Nealey, *ACS Nano*, **2007**, *1*, 168.

[28] C. T. Black, *App. Phys. Lett.*, **2005**, *87*, 163116.

[29] K. L. Killops, N. Gupta, M. D. Dimitriou, N. A. Lynd, H. Jung, H. Tran, J. Bang, and L. M. Campos, *ACS Macro Lett.*, **2012**, *1*, 758.

[30] Yeon Sik Jung, WooChul Jung, Harry L. Tuller and C. A. Ross, *Nano Lett.*, **2008**, *8*, 3776.

[31] J. Y. Cheng, W. Jung, and C. A. Ross, *Phys. Rev. B.*, **2004**, *70*, 064417.

[32] T. Thurn-Albrecht, J. Schotter, G. A. Kästle, N. Emley, T. Shibauchi, L. Krusin-Elbaum, K. Guarini, C. T. Black, M. T. Tuominen, T. P. Russell, *Science*, **2010**, *290*, 2126.

[33] Y.-K. Choi, J. Zhu, J. Grunes, J. Bokor, G. A. Somorjai, *J. Phys. Chem. B*, **2003**, *107*, 3340.

[34] Y. S. Jung, C. A. Ross, *Adv. Mat.*, **2009**, *21*, 2540.

[35] H. Duan, D. Winston, J. K. W. Yang, B. M. Cord, V. R. Manfrinato, and K. K. Berggren, *J. Vac. Sci. & Tech. B*, **2010**, *28*, C6C58.

[36] K. W. Gotrik, A. F. Hannon, J. G. Son, B. Keller, A. Alexander-Katz, and C. A. Ross, *ACS nano*, **2012**, *6*, 8052.

[37] M. W. Matsen and F. S. Bates, *Macromol.*, **1996**, *29*, 1091.

[38] I. W. Hamley, K. A. Koppi, J. H. Rosedale, F. S. Bates, K. Almdal, and K. Mortensen, *Macromol.*, **1993,** *26*, 5959.

[39] S. Foerster, A. K. Khandpur, J. Zhao, F. S. Bates, I. W. Hamley, A. J. Ryan, and W. Bras, *Macromol.*, **1994**, *27*, 6922.

[40] A. K. Khandpur, S. Foerster, F. S. Bates, I. W. Hamley, A. J. Ryan, W. Bras, K. Almdal, and K. Mortensen, *Macromol.*, **1995**, *28*, 8796.

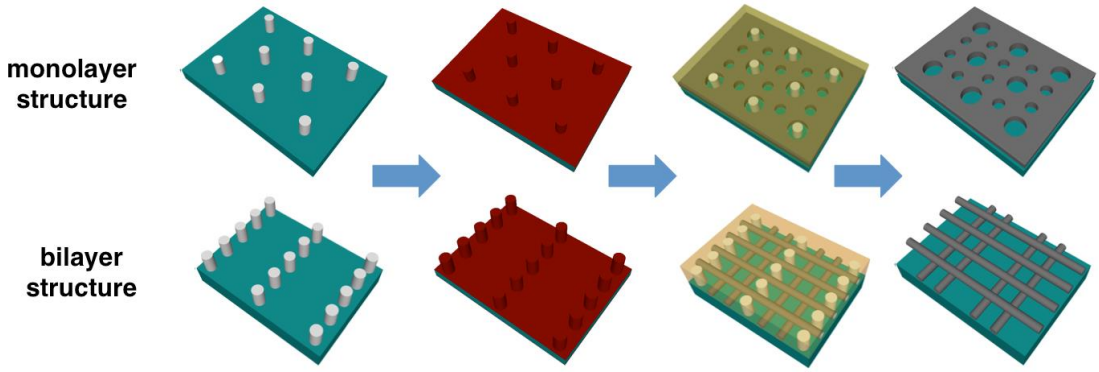

Figure 1: Schematic diagram of the major steps in fabrication of monolayer (top) and bilayer (bottom) microdomain arrays using the sacrificial-post templating method. (Step 1) electron beam lithography fabrication of arrays of posts of negative-tone PMMA resist, (Step 2) functionalization of posts and substrates with a PS brush, (Step 3) spin coating and solvent annealing of the PS-*b*-PDMS BCP thin film, and (Step 4) RIE removal of the top PDMS layer with CF_4 then the PS matrix and PMMA posts with O_2. The ox-PDMS nanostructure remained on the substrates as the final nanopatterns.

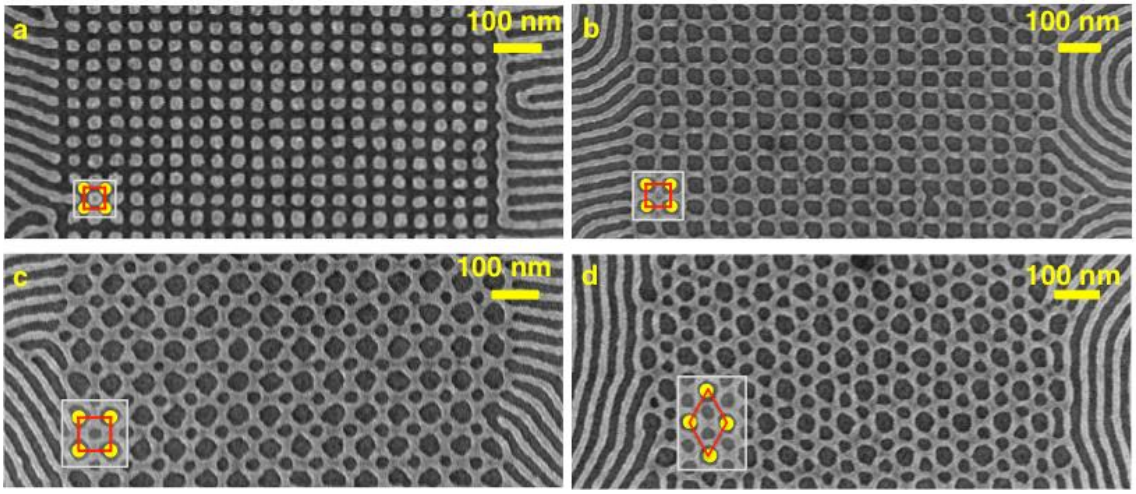

Figure 2: SEMs of monolayer nanostructures fabricated by the sacrificial-post templating method. Shown are a (a) square array of spheres, (b) a square symmetry L1 perforated lamella, (c) square symmetry L2 perforated lamella with one hole generated between each group of four posts and (d) hexagonal symmetry L2 perforated lamella of nanoholes with one hole generated between each group of three posts. Light grey and dark grey colors represent ox-PDMS and the substrate, respectively. Insets show the pre-removal locations of negative-tone PMMA posts in yellow. Red outlines represent unit cells for the final nanostructures. Scale bars are 100 nm.

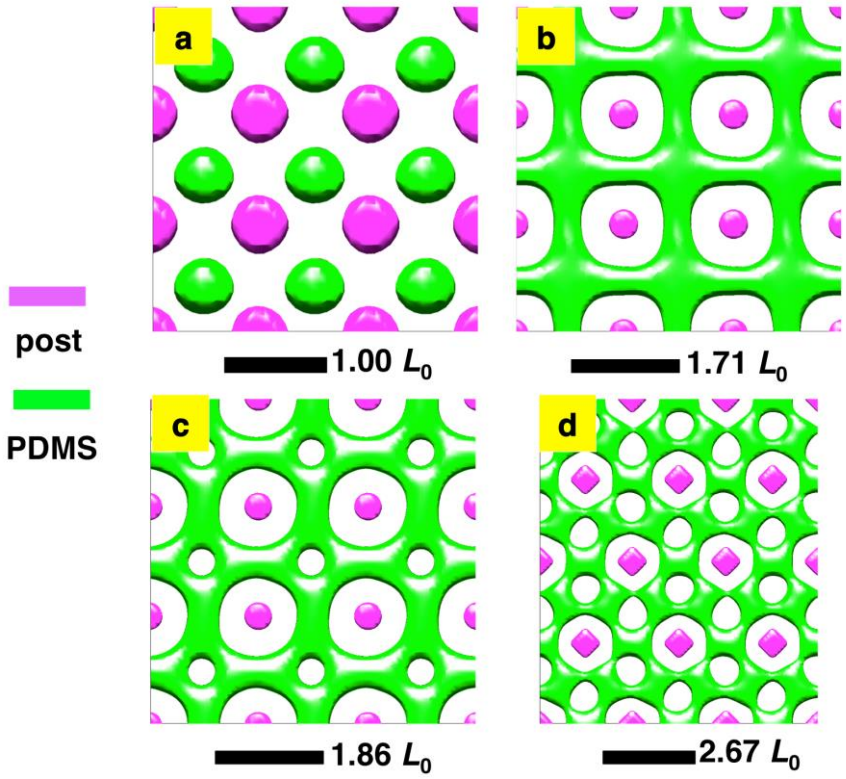

Figure 3: Top-down 3D view of self-consistent field theory simulation results of PS-b-PDMS monolayer thin film equilibrium structures with PS-coated posts of different pitch. (a) A square array of spheres at pitch L_0, (b) a square symmetry perforated lamella L1 for post pitch of 1.71L_0, (c) a square symmetry perforated lamella L2 for pitch 1.86L_0, and (d) a hexagonal symmetry perforated lamella L2 for pitch 2.67L_0. Each image is made as a composite of 9 (a-c) or 6 (d) identical images to show the geometry more clearly. L_0 is the cylinder pitch in the untemplated BCP.

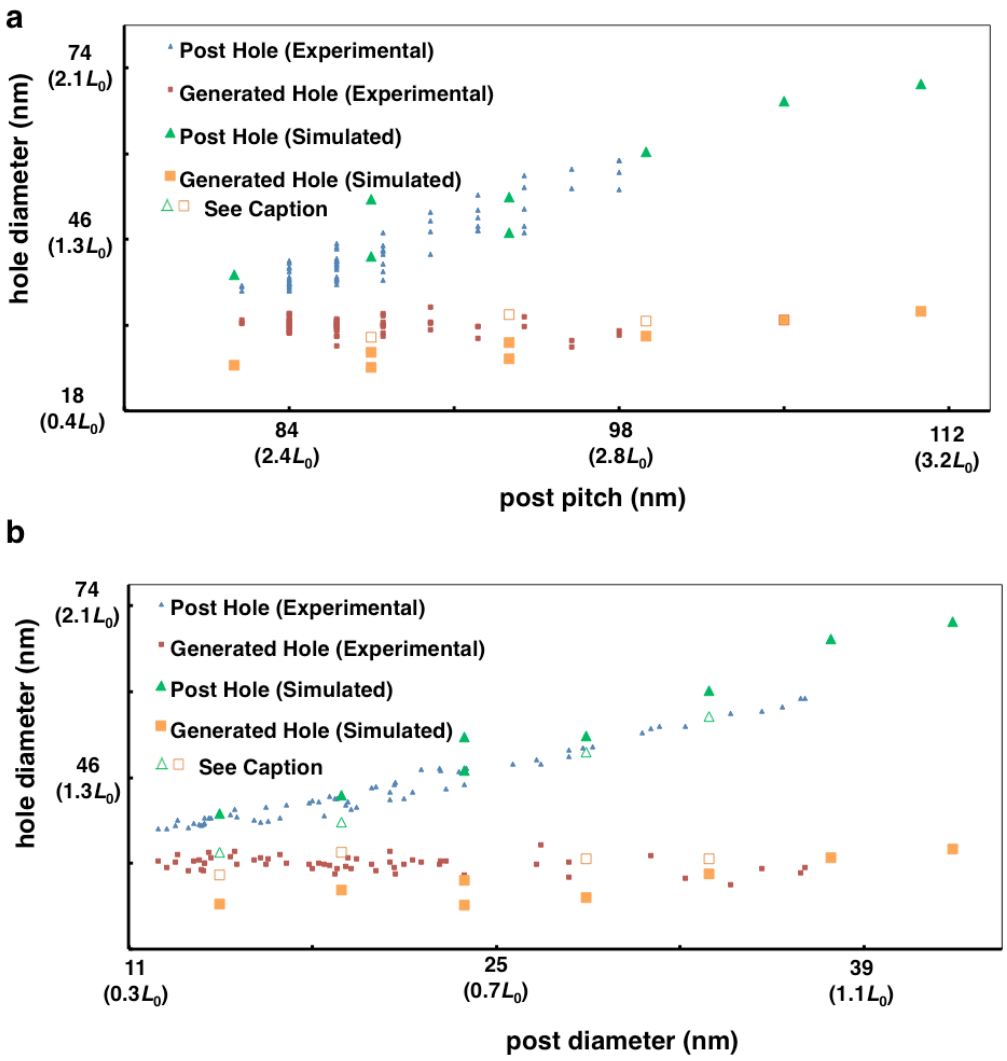

***Figure 4*:** Experimental and simulation graphs of the post-hole and generated-hole diameter versus the (a) post pitch and (b) post diameter. In (a), multiple data points for a given post pitch represent templates with different post diameters. In (b), multiple data points for a given post diameter represent templates with different post pitch. In both simulation and experimental results, the generated-hole diameter does not vary much with post pitch and diameter, whereas the post-hole diameter increases linearly with post pitch and diameter. For experimental data, HSQ posts were used instead of PMMA posts. Open triangles and squares represent structures with defects.

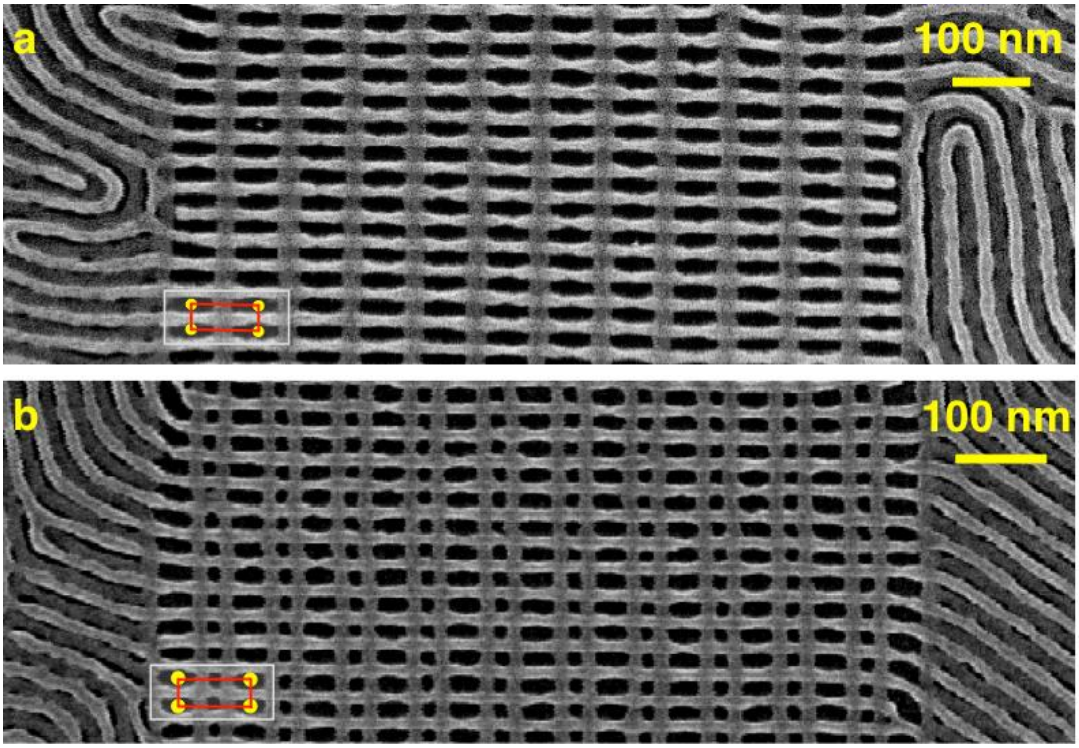

***Figure 5*:** SEMs of mesh structures fabricated by the sacrificial-post templating method. (a) Mesh of rectangular holes from a template with period 35 and 96 nm along the *y* and *x*-directions, respectively; (b) mesh of bimodal rectangular holes from a template with period 36 and 136 nm along the *y* and *x*-directions, respectively. Light grey is the ox-PDMS and dark grey is the substrate. Insets show the locations of negative-tone PMMA posts in yellow. Red outlines represent unit cells for the nanostructures. Scale bars are 100 nm.

The table of contents entry:

The sacrificial post-templating method in block copolymer self-assembly, with the help of majority-block-functionalized posts, achieves several morphologies and structures on a single substrate without template incorporation. This method is applied to direct assembly of a monolayer and bilayer of block copolymer. Arrays of different templates produce square and hexagonal lattices of spheres and perforated lamellae. Furthermore, bimodal hole sizes and density multiplication are achieved. Scale bars are 100 nm.

TOC Keyword:
Sacrificial-post template, block copolymer directed self-assembly, bimodal size distribution, nanostructure, square and hexagonal lattice

S. M. Nicaise, A. F. Hannon, K. W. Gotrik, A. Alexander-Katz, C. A. Ross, K. K. Berggren*

Title: Sacrificial-Post Templating Method for Block Copolymer Self-Assembly

ToC figure:

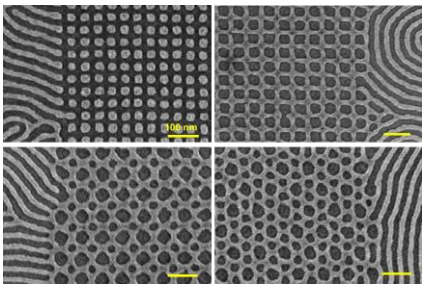

Page Headings
Left page: A. Tavakkoli K. G. et al.
Right page: Sacrificial-Post Templating Method